ADVANCED ENERGY MATERIALS
www.advenergymat.de

The Concept of Negative Capacitance in Ionically Conductive Van der Waals Ferroelectrics

Sabine M. Neumayer, Lei Tao, Andrew O'Hara, Michael A. Susner, Michael A. McGuire, Petro Maksymovych, Sokrates T. Pantelides, and Nina Balke**

Negative capacitance (NC) provides a path to overcome the Boltzmann limit that dictates operating voltages in transistors and, therefore, may open up a path to the challenging proposition of lowering energy consumption and waste heat in nanoelectronic integrated circuits. Typically, NC effects in ferroelectric materials are based on either stabilizing a zero-polarization state or slowing down ferroelectric switching in order to access NC regimes of the free-energy distribution. Here, a fundamentally different mechanism for NC, based on $CuInP_2S_6$, a van der Waals layered ferrielectric, is demonstrated. Using density functional theory and piezoresponse force microscopy, it is shown that an unusual combination of high Cu-ion mobility and its crucial role in determining polarization magnitude and orientation (P) leads to a negative slope of the polarization versus the electric field E, $dP/dE < 0$, which is a requirement for NC. This mechanism for NC is likely to occur in a wide class of materials, offering new possibilities for NC-based devices. The nanoscale demonstration of this mechanism can be extended to the device-level by increasing the regions of homogeneous polarization and polarization switching, for example, through strain engineering and carefully selected electric field pulses.

Dr. S. M. Neumayer, Dr. P. Maksymovych, Dr. N. Balke
Center for Nanophase Materials Sciences
Oak Ridge National Laboratory
Oak Ridge, TN 37831, USA
E-mail: balken@ornl.gov
Dr. L. Tao, Dr. A. O'Hara, Prof. S. T. Pantelides
Department of Physics and Astronomy
Vanderbilt University
Nashville, TN 37235, USA
E-mail: pantelides@vanderbilt.edu
Dr. L. Tao
University of Chinese Academy of Sciences & Institute of Physics
Chinese Academy of Sciences
Beijing 100190, China
Dr. M. A. Susner
Materials and Manufacturing Directorate
Air Force Research Laboratory
Wright-Patterson Air Force Base
Dayton, OH 45433, USA
Dr. M. A. McGuire
Materials Science and Technology Division
Oak Ridge National Laboratory
Oak Ridge, TN 37831, USA
Prof. S. T. Pantelides
Department of Electrical Engineering and Computer Science
Vanderbilt University
Nashville, TN 37235, USA
The ORCID identification number(s) for the author(s) of this article can be found under https://doi.org/10.1002/aenm.202001726.

DOI: 10.1002/aenm.202001726

1. Introduction

Negative capacitance (NC) is a scientific phenomenon that can arise in ferroelectric-based devices. NC provides the intriguing opportunity to operate transistors at voltages below the 60 mV-per-decade limit (a benchmark number to describe current–voltage characteristic of field effect transistors) imposed by the Boltzmann distribution of electrons, allowing for a significant reduction in power consumption and waste heat in electronic devices.[1–9] As a result, NC devices based on ferroelectric materials have attracted significant scientific attention. Such devices, however, are discussed in the context of quasi-static or transient NC phenomena.[10] To understand the various NC approaches, one first considers the definition of capacitance, $C = \frac{dQ}{dV} \propto \frac{dP}{dE}$, where V is the voltage, Q is the charge at the electrode, P is the ferroelectric polarization, and E is the electric field. Therefore, NC is only realized where $\frac{dP}{dE} < 0$, meaning that the polarization change is opposite to the electric-field change. This possibility arises in the thermodynamic regime where the second derivative of the energy-polarization curve is negative as $C = \frac{d^2F}{dP^2}$, where F denotes the free energy[8,11] which is a result of the Landau description for ferroelectric materials.[12,13] In the quasi-static approach, the zero-polarization state around $\frac{d^2F}{dP^2} < 0$ is stabilized by combining the ferroelectric material with a dielectric.[4,9,11] Indeed, it has been shown experimentally at the atomic scale that NC can exist in the steady-state in areas of small dielectric displacement near or at ferroelectric vortex cores in ferroelectric–dielectric heterostructures.[11] In contrast, the transient NC approach is based on accessing the thermodynamically unstable portions of the P–E loop where the zero-polarization state is passed.[8,14,15] The inherently unstable nature of this state can be experimentally overcome by slowing down switching dynamics via the addition of a large resistor or resistive material to the electronic circuit. Other concepts to access the NC regime are based on ferroelectric nanodot capacitors in a two-domain ground state, where the ratio of domains can modify the $Q(V)$ dependence.[6] However, only small parts of the negative capacitance regime can be accessed in these examples. Moreover, alternative explanations for the experimentally observed voltage drop during an increase in charge have been suggested and include dead layers, changes in resistance,

domain formation, and nonlinear positive capacitance.[16–19] Therefore, the experimental observation of NC in ferroelectric materials remains a challenge and is presently under debate.

Copper indium thiophosphate, $CuInP_2S_6$ (CIPS), a van der Waals (vdW) layered material that is ferrielectric at room temperature[20–24] has been explored for NC due to its compatibility with other 2D materials for advanced heterostructures.[25] The polarization of CIPS arises from the noncentrosymmetric z displacement of Cu and In atoms with respect to the P_2S_6 sublattice.[26,27] Recently, density functional theory (DFT) demonstrated the presence of two iso-symmetric polar phases.[28] When the Cu ions reside within the layers, the predicted polarization is ≈5 μC cm^{-2} (termed the low polarization or LP phase) whereas if Cu occupies sites within the vdW gaps, the spontaneous polarization is predicted to double to ≈11 μC cm^{-2} (termed the high polarization or HP phase). Both phases are aligned either parallel (+) or antiparallel (−) to z, resulting in a quadruple-well energy potential as a function of Cu z displacement instead of the usual double-well potential. The calculated piezoelectric constants for the two polar phases enabled the experimental verification of these phases by piezoresponse force microscopy (PFM) measurements of the piezoelectric constants. Moreover, the material also exhibits giant negative electrostrictive coefficients,[24,29] which is a direct consequence of the highly anharmonic potential well.[28] In addition, CIPS has a high Cu-ion conductivity that extends into the temperature range of the ferroelectric phase.[30–32] It has been shown that in-plane ionic currents can be used to manipulate ferroelectric polarization.[33] These highly unusual properties that are rooted in the vdW structure provide the opportunity for complex polarization switching which might be exploited in transient-NC devices beyond the mechanisms discussed above.

In this paper, we identify a unique mechanism for NC enabled by the vdW gap and the high Cu-ion mobility. The symmetries of the CIPS structure reveal and DFT calculations confirm two centrosymmetric Cu sites, one in the mid-plane of the layers and the second in the mid-plane of the vdW gaps where the polarization is zero. The Cu-ion conductivity of CIPS under electric fields E confirms the ability of Cu ions to move through both the layers and the vdW gaps, which requires that some regions in the Cu migration path exhibit $dP/dE < 0$ due to the two iso-symmetric planes with zero polarization. Indeed, DFT calculations find that, as the Cu ions move in the $+z$ direction under an externally applied electric field E, the polarization P increases from a large negative value to a large positive value when they cross the layers, while it decreases from the large positive value to a large negative value when they cross the vdW gaps. The latter phenomenon results in a polarization alignment against the applied electric field and $dP/dE < 0$, signaling a mechanism for NC. In order to experimentally verify that this highly unusual polarization alignment does indeed occur, we use PFM to measure d-E hysteresis loops, where d is the piezoelectric coefficient. Combining these measurements with experimentally validated theoretical, $d(P)$ values,[28] we derive local P-E hysteresis loops. We observe local regions on 20–200 nm length scales with polarization transitions in agreement with the theoretical predictions of polarization reversal against the electric field during ionic motion through the vdW gaps, which results in P-E loops with a negative slope as required for effective NC. This mechanism can contribute to transient negative capacitance in ways that are distinctively different from previously proposed mechanisms where only thermodynamically unstable parts of the P-E loop yield negative capacitance and suggest a new paradigm for the realization of NC devices. In this work, we demonstrate the NC polarization transition mechanism for nanoscale regions, whereas device-level applications demand larger domains that exhibit a specific switching pathway. We envision that strain engineering and targeted voltage pulses can be employed to achieve this goal, however, further studies will be necessary. Moreover, the NC regime is tied to the process of polarization switching, during which lower operating voltages of field effect transistors might be achieved.

2. Results and Discussion

The quadruple-well in CIPS was discovered using DFT calculations by moving the Cu ions beyond their first total-energy minimum, revealing a second minimum originating from a second polar phase.[28] As a next step, we now explore the energy landscape when the Cu ions are displaced along the z axis beyond the layers and across the vdW gaps (**Figure 1**a). Indeed, it has been shown experimentally that Cu ions can cross individual vdW gaps in CIPS under the influence of an electric field.[34] For each Cu position, DFT is used to calculate the total energy as well as the polarization. As noted already, due to the symmetry of CIPS, there are two zero-polarization states: when the Cu ions are a) in planes at the mid-points of the layers and b) in planes at the mid-points of the vdW gaps. This feature results in two polarization curves calculated relative to the corresponding zero-polarization planes as reference points (Figure S1, Supporting Information). The crossover of the two polarization curves is used as the transition from one curve to the other curve to yield a single continuous curve. The total energy and the corresponding polarization across two layers and the in-between vdW gap are shown in Figure 1b,c, respectively. The four possible polarization states in CIPS, ±LP and ±HP, are indicated. The energy barrier for Cu ions to cross the vdW gap is calculated to be ≈0.6 eV, which fits well in the range of reported activation barriers for Cu-ion conduction[32,35] and can be easily overcome using electric fields. If the Cu ions move beyond the unit cell and across the vdW gap along the z axis under the influence of an electric field, the resulting polarization exhibits unusual behavior. Whereas the polarization increases in the direction of the electric field when the Cu ions move across the layers, the polarization is reduced when the Cu ions move under the influence of the same electric field across the vdW gap, going through zero at the mid-gap point (Figure 1c). If we can control the position of Cu with electric fields, $z(E)$, then we can write $\frac{dP}{dE} = \frac{dP}{dz}\cdot\frac{dz}{dE}$. Since the Cu displacement z is always in the direction of E, dz/dE is always positive and the sign of dP/dz (Figure 1c) indicates the sign of dP/dE. Therefore, the Cu jump across the vdW gap fits the definition of negative capacitance. Note that this process is not linked to the existence of the quadruple energy well in CIPS, but can be generalized to double-well ferroelectrics as well if the atoms that are linked to polar displacements face reasonable barriers into the adjacent unit cell. In oxide ferroelectrics, the atomic

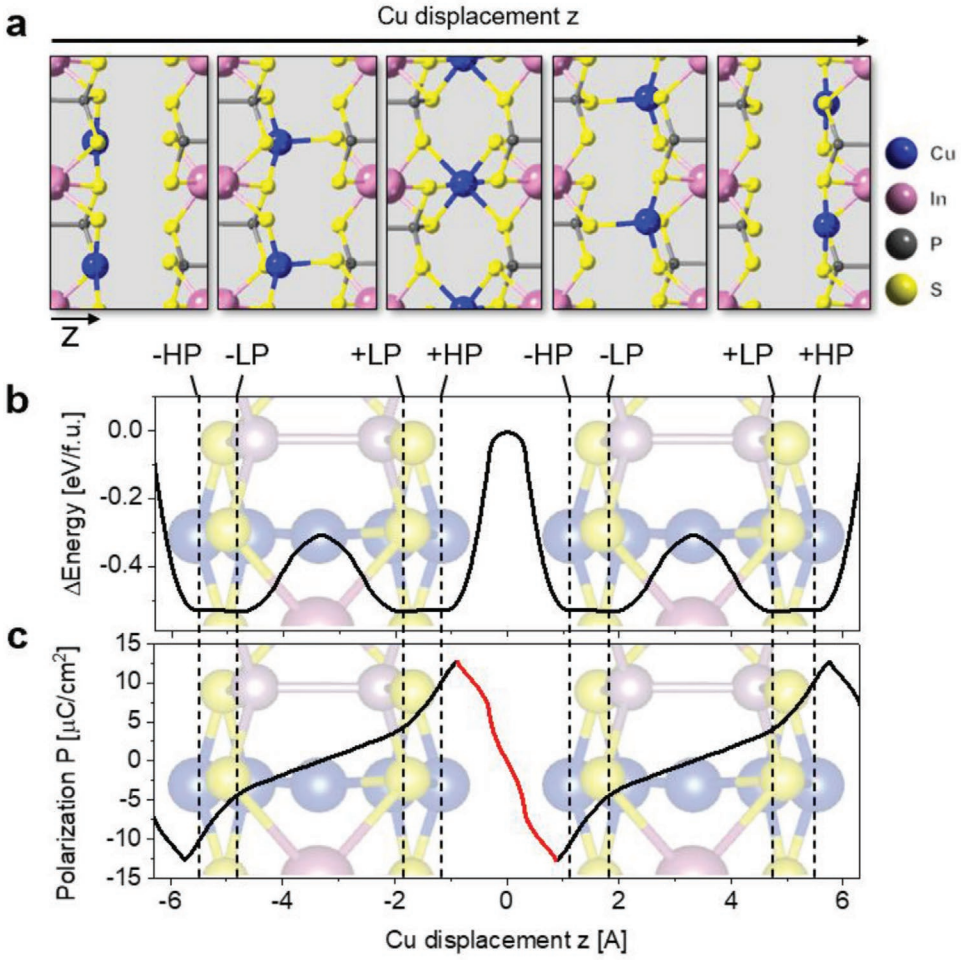

Figure 1. a) Structural image sequence when Cu atoms cross the vdW gap. Total energy b) as well as polarization c) as function of Cu displacement across two layers and one gap. The background in b) and c) is a composite image of different Cu position schematically illustrating the Cu moving through the layers. The red line indicates the predicted regime of negative capacitance where $\frac{dP}{dE} \propto \frac{dP}{dz} < 0$.

species that is responsible for polar displacements is not mobile enough to move into the next unit cell due to high energy barriers, whereby we do not expect this phenomenon to occur. However, in the case of ferroelectric ion conductors, such as CIPS, this scenario is likely if an electric field is applied that is sufficient to induce ionic conduction. In fact, Scott has proposed that sufficiently large voltages may enable a transition from ferroelectric switching to ion conduction in some ferroelectric ion conductors such as $Ag_{26}I_{18}W_4O_{16}$ and CsH_2PO_4.[36] Therefore, we believe this mechanism is not restricted to CIPS but is a general phenomenon in ferroelectric ion conductors. There is no negative capacitance regime around the zero-polarization state within the CIPS layers.

We highlight that this approach is necessitated by the interplay of polar properties and ion conduction and fundamentally distinct from the Landau-based thermodynamic description of the ferroelectric polarization switching process.[12,13]

In the following, we explore if $dP/dE < 0$ can be observed experimentally in CIPS. We are interested in length scales corresponding to the sizes of the polarization domains in CIPS (tens to hundreds of nm across); at these dimensions, the polarization cannot be directly measured. Instead, we utilize the direct link between piezoelectric constant and polarization established by DFT[28] allowing for a direct probing of polarization using local probes. Local probes enable us to access and analyze the switching pathways of individual domains in CIPS, unlike typical *P-E* measurements on capacitors where averaging across large areas might obfuscate details in switching dynamics. In order to monitor the piezoelectric constant under applied electric fields, we performed PFM voltage spectroscopy.[37] When correctly calibrated and quantified, the PFM response measures the piezoelectric constant along the surface normal, here, closest linked to d_{33} or simply d. However, knowledge of non-piezoelectric signal contributions such as electrostatic forces is required to avoid artifacts. We, therefore, performed PFM voltage spectroscopy on a two-phase sample containing two separate chemical phases of ferrielectric CIPS and non-piezoelectric $In_{4/3}P_2S_6$ (IPS). This phase separation is achieved by synthesizing an off-stochiometric composition ($Cu_{0.4}In_{1.2}P_2S_6$) which results in the separation into a fully stochiometric CIPS phase and a non-Cu containing IPS phase.[38] The map of local d values for CIPS domains at zero field can be seen in **Figure 2**a,

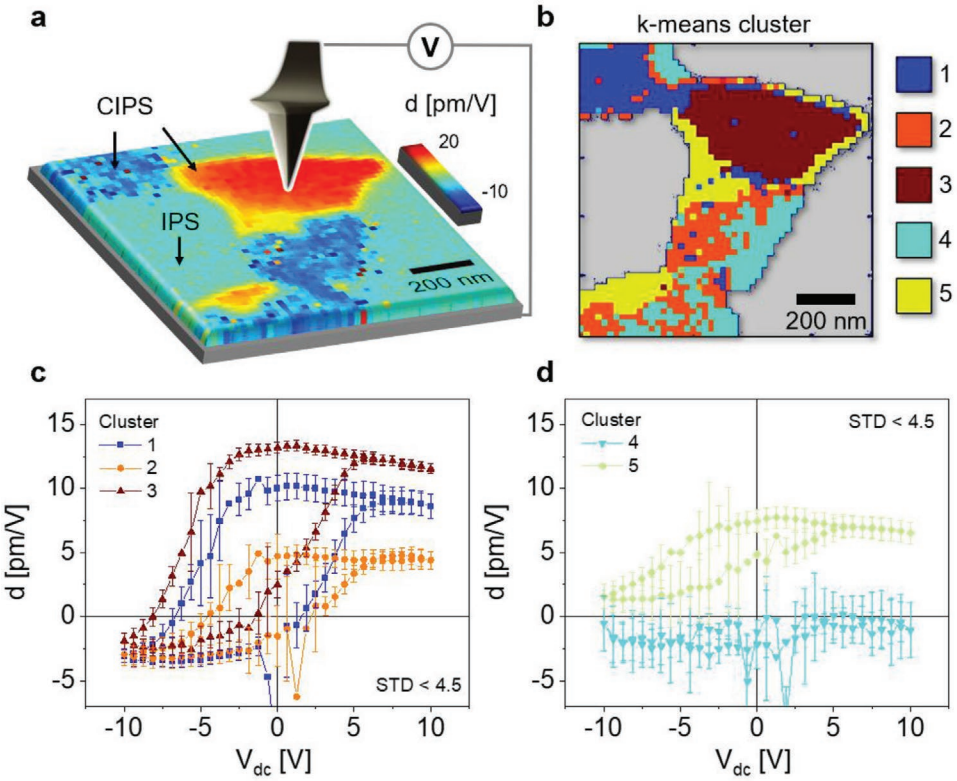

Figure 2. a) Quantified PFM image of a $1 \times 1\ \mu m^2$ area showing ferroelectric CIPS and non-ferroelectric IPS and schematic setup. b) k-means cluster map of the voltage-dependent change of d showing five clusters. c) Averaged piezoelectric hysteresis for clusters 1–3 and d) 4 and 5. Since the error bars are artificially enhanced when the SHO data fit fails around low-response regions, only standard variations which fall within 4.5 pm V^{-1} are shown. This value was determined by looking at the histogram of all standard deviations (Figure S3a, Supporting Information). The hysteresis loops with all error bars are shown in Figure S3b–f, Supporting Information.

which shows distinct ferroelectric domains and a zero response IPS phase. During voltage spectroscopy, the voltage was varied between ±10 V and the change in piezoelectric constant was detected spatially resolved on a 50×50 grid. Based on the PFM image, the CIPS and IPS phases can be separated and analyzed individually (Figure S2a,b, Supporting Information). The relative area fractions of CIPS and IPS are 0.492 and 0.508, respectively. Since the local Cu content is only determined by the area fraction of CIPS and the local In content is determined by the area fraction of CIPS (contributes 1 In per formula unit) and the area fraction of IPS (contributes 4/3 In per formula unit), the local composition can be estimated to be $Cu_{0.49}In_{1.16}P_2S_6$ which is slightly higher in Cu content than the macroscopic composition.

While CIPS shows a hysteretic loop with significantly small error bars when averaged over the CIPS phase (Figure S2c, Supporting Information), the IPS response is mostly linear indicating electrostatic signal contributions (Figure S2d, Supporting Information).[39] The lack of hysteresis suggests no charge injection from the tip as observed in other non-ferroelectric phases.[40] By subtracting the response measured on IPS from the one on CIPS, non-electromechanical contributions to the PFM signal can be eliminated for CIPS areas.

The large signal variation in the averaged CIPS hysteresis loop (Figure S2c, Supporting Information) originates from local variations that are analyzed using k-means clustering which is a standard analysis tool that allows the partitioning of data into n clusters, where every cluster is represented by a prototype data set.[41] Five distinct behavior types can be identified (Figure 2b). Clusters 1–3 occupy the centers of the domains and show clear hysteresis loops with remanent values (Figure 2c), whereas clusters 4 and 5 occur mostly at the CIPS/IPS interface and do not show well-developed hysteresis (Figure 2d). We attribute the underdeveloped hysteresis loops to clamping effects by the neighboring IPS phase which has a smaller layer spacing and can impose strain on CIPS depending on the Cu/In ratio.[42] Therefore, we believe that the ferroelectric switching process is affected by the local sample composition, that is, the local amount of IPS phase.

DFT calculations recently predicted the piezoelectric constants for the two polar phases in CIPS to be –15.6 pm V^{-1} for +LP and +2.6 pm V^{-1} for +HP and these values were experimentally verified using PFM.[28] The corresponding negative orientations –LP and –HP would be measured as +15.6 pm V^{-1} and –2.6 pm V^{-1}, respectively. Therefore, based on the sign and amplitude of the measured piezoelectric constants, the polarization states can be uniquely identified from the measured d values. The distribution of d values at zero dc voltage (0 V_{dc}) for the hysteretic clusters 1–3 shows three unique signal levels corresponding to three peaks (**Figure 3**a). Note that every cluster contributes to two different value distributions due to the presence of two different remnant values after application of negative or positive voltages which is shown in detail in

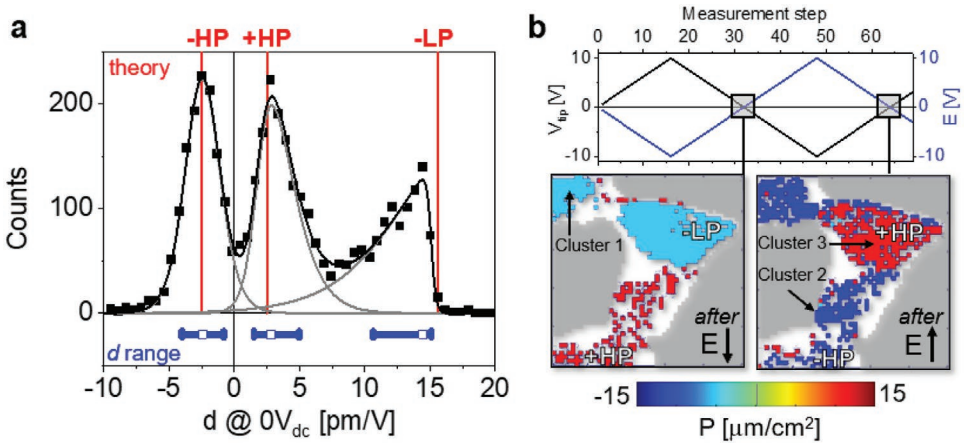

Figure 3. a) Histogram of remanent values of *d* for switching clusters 1–3 which are fitted by bi-Gaussian curves to extract the full width half maxima which are shown as horizontal blue lines (*d* range). The theoretically predicted values of *d* are indicated as red vertical lines for three polarization states. b) Remanent polarization phase map after the application of negative fields and positive fields, respectively.

Figure S4, Supporting Information. When compared to theoretical predictions, the three signal levels can be assigned to the –HP, +HP, and –LP polarization states, respectively. We assign the width of the experimental peaks to small local data variations as well as data noise. We used the asymmetric full width at half maximum of each distribution peak to set boundaries for polarization phase classification and applied this procedure to all measured *d* values for every applied voltage to obtain polarization curves from *d* for clusters 1–3.

When plotting the remanent polarization states assigned by the above-described procedure, we can see that after the application of positive voltages to the tip (or negative fields across CIPS), –LP and +HP polarization states can be found, whereas after the application of negative voltages to the tip (or positive fields across CIPS), –HP and +HP polarization states are present (Figure 3b). In cluster 1, we observe a –LP↔–HP phase transition without polarization direction change. In cluster 3, the remanent polarization orientation follows the direction of the applied electric field, as expected for a ferroelectric material. After the application of negative fields, we observe the –LP state and after applying positive fields we observe the +HP state. In comparison to regular ferroelectrics, this cluster describes a phase transition and a polarization reversal enabled by the quadruple potential well. In the region occupied by cluster 2, we can identify a new type of polarization reversal, which is uncommon for traditional ferroelectrics where the polarization aligns against the electric field direction. After the application of negative fields, we observe a positive polarization state (+HP) and after the application of positive fields, we observe a negative polarization state (–HP). After assigning polarization states according to Figure 3a, the polarization curve as well as its derivative for cluster 2 is shown in **Figure 4**. The derivative of the polarization curve $\frac{dP}{dE}$ is negative, which is necessary to realize negative capacitance.

The polarization loops shown in Figure 4 look like ferroelectric *P-E* loops but with reversed orientations. These loops cannot be understood in the context of dipole reorientation but only in the context of ionic transport across the vdW gap. Figure 4a demonstrates that it is possible to isolate the transition between the two HP states, equivalent to a jump of the Cu ions across the vdW gaps, and to do so reversibly. This possibility is evident from the good match between subsequent hysteresis loops (Figure S5a, Supporting Information) and the same PFM images before and after the measurement (Figure S5b,

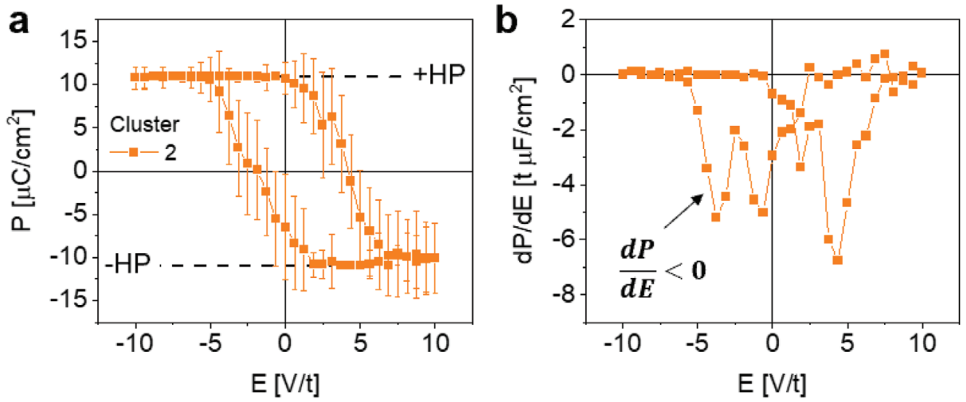

Figure 4. a) Averaged polarization hysteresis loop and b) derivative for cluster 2. The region of negative slope in the derivative curves is indicated by an arrow.

Supporting Information). Therefore, we can conclude that ionically driven polarization loops form the basis of a new NC mechanism with negative dP/dE. To isolate the Cu jump across the vdW gap, the timing of the hysteresis loop frequency needs to be just right since faster measurements would not allow Cu ions to cross the vdW gap and slower measurements would result in Cu ions crossing gaps and layers and the net effect might not result in the desired polarization transition. The exact mechanism how the Cu ions cross the vdW gap and how these crossings transform the bias-dependent energy landscape is presently unclear and subject to further studies.

We note that we only observe the NC polarization transition in a sub-domain area and domain engineering as well as active modification of switching pathways would need to be achieved before the proposed mechanism can be harnessed in a device setting. We propose that this should be possible through strain and targeted voltage pulses applied to modify the local Cu environment. It will also be important to understand the role of surfaces in the observed switching pathways since surfaces limit the available positions for Cu atoms. The interplay between ferroelectric and ionic properties is highly complex and strongly depends on temperature, voltage pulse amplitudes, and durations. If voltages are applied over long time scales, long-range ion migration occurs and leads to the buildup of space charge layers under the electrodes leading to significant modification of polarization loops.[31]

3. Conclusions

In conclusion, we have discovered an alternative mechanism to access negative capacitance $C = \frac{dP}{dE} < 0$ using vdW layered ferroelectric materials. First, we theoretically describe and experimentally verify stable *P-E* loops with negative slope attributed to the crossing of Cu ions across the vdW gaps under the influence of an applied field. In this case, the alignment of the polarization is anti-parallel to the electric field, which is in stark contrast to conventional ferroelectric behavior, where the permanent dipoles rotate to align with the electric field. We have shown experimentally that, locally, this process is reversible, resulting in reproducible polarization hysteresis loops. This phenomenon is not likely to be restricted to CIPS, but should happen in all ferroelectric materials with high ionic conductivity on the same atomic sub-lattice, especially layered ferroelectrics that can sustain such ionic conductivity. Therefore, CIPS and related classes of materials could provide a new outlook on harnessing negative capacitance. The realization of macroscopic devices to utilize these new forms of polarization control requires domain engineering and the understanding of the role of local strains.

4. Experimental Section

Crystal Synthesis: Single crystals of $CuInP_2S_6$ were synthesized using the vapor transport method, as previously described.[38] In short, starting materials (Cu, S, P, and In_2S_3) were sealed in fused silica ampoules and reacted at 750–775 °C for 96 h., after which point, they were cooled to room temperature at a rate of 20 °C h^{-1}. Final bulk compositions of the crystals were determined by a Hitachi TM-3000 scanning electron microscope mated with a Bruker Quantax 70 energy dispersive X-ray spectrometer. The composition was determined to be $Cu_{0.42(6)}In_{1.23(5)}P_{2.06(5)}S_6$ and phase identification was confirmed with X-ray diffraction as reported in Susner et al.[38]

Theory: The DFT calculations in this study were performed with the Vienna Ab-initio Simulation Package (VASP)[43] where the core–valence–electron interactions were described via the projected-augmented-wave (PAW) method.[44,45] The wave functions were expanded in a plane-wave basis using a 600 eV energy cutoff. Exchange and correlation effects were described using the Perdew–Burke–Ernzerh[46] generalized gradient approximation including van der Waals corrections via Grimme's DFT-D3 method with Becke–Johnson (BJ) damping.[47,48] All calculations use a Γ-centered Monkhorst–Pack (MP) k-point grid[49] of $4 \times 4 \times 4$. At each step of the calculations, the Cu *z*-displacement is kept fixed by freezing the *z*-coordinates of the Cu and one P atom per dipole, while all other atoms are relaxed until the net force is less than 0.01 eV $Å^{-1}$. The polarization is obtained by the modern theory of polarization based on the Berry-phase approach.[50,51]

Experimental: The measurements were performed on a single mm-sized crystal with a thickness of 100s of micrometers in a flat region on the crystal surface. The sample was attached by silver paint to the microscopy stage which serves as an electric back contact. The PFM tip serves as local variable electrode and all voltages are applied to the PFM tip. The sample was cleaved using Scotch tape directly before the measurement. PFM voltage spectroscopy[37] was performed using a Bruker Icon atomic force microscope in an Ar filled environment. A nanosensor PPP-EFM probe (nominal resonance frequency 75 kHz, nominal force constant 2.8 N m^{-1}) was used. Alternating current voltages of 1 V amplitude were applied in a frequency band around contact resonance with 320 ± 35 kHz to detect the piezoresponse of the sample. During voltage spectroscopy, direct current voltages were swept in a pulsed triangular sequence between +10 and −10 V and the resulting electromechanical response was recorded for a grid of 50×50 pixels within a 1×1 μm^2 area. The effective frequency of the triangular voltage waveform is about 2 Hz. On every pixel, three hysteresis loops were measured and averaged over the 2nd and 3rd cycle. The direct link between piezoelectric constant and polarization (determined by Cu position) established by DFT[28] allows for a direct probing of Cu position using local probes.

Supporting Information

Supporting Information is available from the Wiley Online Library or from the author.

Acknowledgements

The experimental work as well as part of the data analysis and interpretation were supported by the U.S. Department of Energy, Office of Science, Basic Energy Sciences, Materials Science and Engineering Division. Theory was supported by the U.S. Department of Energy, Office of Science, Division of Materials Science and Engineering under Grant No. DE-FG02-09ER46554 and by the McMinn Endowment at Vanderbilt University. The experiments were conducted at the Center for Nanophase Materials Sciences, which is a DOE Office of Science User Facility. Calculations were performed at the National Energy Research Scientific Computing Center, a DOE Office of Science User Facility supported by the Office of Science of the U.S. Department of Energy under Contract No. DE-AC02-05CH11231. Manuscript preparation was partially funded by the Air Force Research Laboratory under an Air Force Office of Scientific Research grant (LRIR Grant No. 19RXCOR052).

Conflict of Interest

The authors declare no conflict of interest.

Keywords

$CuInP_2S_6$, density functional theory, negative capacitance, piezoresponse force microscopy, van der Waals

Received: May 22, 2020
Revised: August 20, 2020
Published online:

[1] E. Ko, J. Shin, C. Shin, *Nano Convergence* **2018**, *5*, 2.
[2] P. Zubko, G. Catalan, A. K. Tagantsev, *Annu. Rev. Mater. Res.* **2013**, *43*, 387.
[3] M. Si, C. J. Su, C. Jiang, N. J. Conrad, H. Zhou, K. D. Maize, G. Qiu, C. T. Wu, A. Shakouri, M. A. Alam, P. D. Ye, *Nat. Nanotechnol.* **2018**, *13*, 24.
[4] W. Gao, A. Khan, X. Marti, C. Nelson, C. Serrao, J. Ravichandran, R. Ramesh, S. Salahuddin, *Nano Lett.* **2014**, *14*, 5814.
[5] M. Hoffmann, M. Pesic, S. Slesazeck, U. Schroeder, T. Mikolajick, *Nanoscale* **2018**, *10*, 10891.
[6] I. Lukyanchuk, Y. Tikhonov, A. Sene, A. Razumnaya, V. M. Vinokur, *Comm. Phys.* **2019**, *2*, 22.
[7] V. V. Zhirnov, R. K. Cavin, *Nat. Nanotechnol.* **2008**, *3*, 77.
[8] A. I. Khan, K. Chatterjee, B. Wang, S. Drapcho, L. You, C. Serrao, S. R. Bakaul, R. Ramesh, S. Salahuddin, *Nat. Mater.* **2015**, *14*, 182.
[9] S. Salahuddin, S. Datta, *Nano Lett.* **2008**, *8*, 405.
[10] M. A. Alam, M. Si, P. D. Ye, *Appl. Phys. Lett.* **2019**, *114*, 090401.
[11] A. K. Yadav, K. X. Nguyen, Z. Hong, P. Garcia-Fernandez, P. Aguado-Puente, C. T. Nelson, S. Das, B. Prasad, D. Kwon, S. Cheema, A. I. Khan, C. Hu, J. Iniguez, J. Junquera, L. Q. Chen, D. A. Muller, R. Ramesh, S. Salahuddin, *Nature* **2019**, *565*, 468.
[12] M. E. Lines, A. M. Glass, *Principles and Applications of Ferroelectrics and Related Materials*, Oxford University Press, Oxford **2001**.
[13] M. Hoffmann, A. I. Khan, C. Serrao, Z. Lu, S. Salahuddin, M. Pešić, S. Slesazeck, U. Schroeder, T. Mikolajick, *J. Appl. Phys.* **2018**, *123*, 184101.
[14] J. Jo, W. Y. Choi, J. D. Park, J. W. Shim, H. Y. Yu, C. Shin, *Nano Lett.* **2015**, *15*, 4553.
[15] A. I. Khan, K. Chatterjee, J. P. Duarte, Z. Lu, A. Sachid, S. Khandelwal, R. Ramesh, C. Hu, S. Salahuddin, *IEEE Electron Device Lett.* **2016**, *37*, 111.
[16] A. K. Saha, S. Datta, S. K. Gupta, *J. Appl. Phys.* **2018**, *123*, 105102.
[17] Y. J. Kim, H. W. Park, S. D. Hyun, H. J. Kim, K. D. Kim, Y. H. Lee, T. Moon, Y. B. Lee, M. H. Park, C. S. Hwang, *Nano Lett.* **2017**, *17*, 7796.
[18] S. J. Song, Y. J. Kim, M. H. Park, Y. H. Lee, H. J. Kim, T. Moon, K. Do Kim, J. H. Choi, Z. Chen, A. Jiang, C. S. Hwang, *Sci. Rep.* **2016**, *6*, 20825.
[19] A. Islam Khan, D. Bhowmik, P. Yu, S. Joo Kim, X. Pan, R. Ramesh, S. Salahuddin, *Appl. Phys. Lett.* **2011**, *99*, 113501.
[20] A. Simon, J. Ravez, V. Maisonneuve, C. Payen, V. B. Cajipe, *Chem. Mater.* **1994**, *6*, 1575.
[21] A. Grzechnik, V. B. Cajipe, C. Payen, P. F. McMillan, *Solid State Commun.* **1998**, *108*, 43.
[22] X. Bourdon, A. R. Grimmer, V. B. Cajipe, *Chem. Mater.* **1999**, *11*, 2680.
[23] A. Belianinov, Q. He, A. Dziaugys, P. Maksymovych, E. Eliseev, A. Borisevich, A. Morozovska, J. Banys, Y. Vysochanskii, S. V. Kalinin, *Nano Lett.* **2015**, *15*, 3808.
[24] F. Liu, L. You, K. L. Seyler, X. Li, P. Yu, J. Lin, X. Wang, J. Zhou, H. Wang, H. He, *Nat. Commun.* **2016**, *7*, 12357.
[25] X. Wang, P. Yu, Z. Lei, C. Zhu, X. Cao, F. Liu, L. You, Q. Zeng, Y. Deng, C. Zhu, J. Zhou, Q. Fu, J. Wang, Y. Huang, Z. Liu, *Nat. Commun.* **2019**, *10*, 3037.
[26] V. Maisonneuve, V. Cajipe, A. Simon, R. Von Der Muhll, J. Ravez, *Phys. Rev. B* **1997**, *56*, 10860.
[27] M. A. Susner, M. Chyasnavichyus, M. A. McGuire, P. Ganesh, P. Maksymovych, *Adv. Mater.* **2017**, *29*, 1602852.
[28] J. A. Brehm, S. M. Neumayer, L. Tao, A. O'Hara, M. Chyasnavichus, M. A. Susner, M. A. McGuire, S. V. Kalinin, S. Jesse, P. Ganesh, S. T. Pantelides, P. Maksymovych, N. Balke, *Nat. Mater.* **2020**, *19*, 43.
[29] S. M. Neumayer, E. A. Eliseev, M. A. Susner, A. Tselev, B. J. Rodriguez, J. A. Brehm, S. T. Pantelides, G. Panchapakesan, S. Jesse, S. V. Kalinin, M. A. McGuire, A. N. Morozovska, P. Maksymovych, N. Balke, *Phys. Rev. Mater.* **2019**, *3*, 024401.
[30] J. Banys, J. Macutkevic, V. Samulionis, A. Brilingas, Y. Vysochanskii, *Phase Transitions* **2004**, *77*, 345.
[31] S. Zhou, L. You, A. Chaturvedi, S. A. Morris, J. S. Herrin, N. Zhang, A. Abdelsamie, Y. Hu, J. Chen, Y. Zhou, S. Dong, J. Wang, *Mater. Horiz.* **2020**, *7*, 263.
[32] N. Balke, S. M. Neumayer, J. A. Brehm, M. A. Susner, B. J. Rodriguez, S. Jesse, S. V. Kalinin, S. T. Pantelides, M. A. McGuire, P. Maksymovych, *ACS Appl. Mater. Interfaces* **2018**, *10*, 27188.
[33] D.-D. Xu, R.-R. Ma, Y.-F. Zhao, Z. Guan, Q.-L. Zhong, R. Huang, P.-H. Xiang, N. Zhong, C.-G. Duan, *J. Mater. Chem. C* **2020**, *8*, 6966.
[34] S. M. Neumayer, L. Tao, A. O'Hara, J. Brehm, M. Si, P.-Y. Liao, T. Feng, S. V. Kalinin, P. D. Ye, S. T. Pantelides, P. Maksymovych, N. Balke, *Phys. Rev. Appl.* **2020**, *13*, 064063.
[35] V. Maisonneuve, J. M. Reau, M. Dong, V. B. Cajipe, C. Payen, J. Ravez, *Ferroelectrics* **1997**, *196*, 257.
[36] J. F. Scott, *Solid State Ionics* **1999**, *125*, 141.
[37] S. Jesse, A. P. Baddorf, S. V. Kalinin, *Appl. Phys. Lett.* **2006**, *88*, 062908.
[38] M. A. Susner, M. Chyasnavichyus, A. A. Puretzky, Q. He, B. S. Conner, Y. Ren, D. A. Cullen, P. Ganesh, D. Shin, H. Demir, J. W. McMurray, A. Y. Borisevich, P. Maksymovych, M. A. McGuire, *ACS Nano* **2017**, *11*, 7060.
[39] N. Balke, S. Jesse, P. Yu, B. Carmichael, S. V. Kalinin, A. Tselev, *Nanotechnology* **2016**, *27*, 425707.
[40] N. Balke, P. Maksymovych, S. Jesse, A. Herklotz, A. Tselev, C.-B. Eom, I. I. Kravchenko, P. Yu, S. V. Kalinin, *ACS Nano* **2015**, *9*, 6484.
[41] A. Belianinov, R. Vasudevan, E. Strelcov, C. Steed, S. M. Yang, A. Tselev, S. Jesse, M. Biegalski, G. Shipman, C. Symons, A. Borisevich, R. Archibald, S. Kalinin, *Adv. Struct. Chem. Imaging* **2015**, *1*, 6.
[42] M. A. Susner, A. Belianinov, A. Borisevich, Q. He, M. Chyasnavichyus, H. Demir, D. Sholl, P. Ganesh, D. Abernathy, M. A. McGuire, P. Maksymovych, *ACS Nano* **2015**, *9*, 12365.
[43] G. Kresse, J. Furthmüller, *Phys. Rev. B* **1996**, *54*, 11169.
[44] G. Kresse, D. Joubert, *Phys. Rev. B* **1999**, *59*, 1758.
[45] P. E. Blöchl, *Phys. Rev. B* **1994**, *50*, 17953.
[46] J. P. Perdew, K. Burke, M. Ernzerhof, *Phys. Rev. Lett.* **1996**, *77*, 3865.
[47] A. D. Becke, E. R. Johnson, *J. Chem. Phys.* **2005**, *123*, 154101.
[48] S. Grimme, S. Ehrlich, L. Goerigk, *J. Comput. Chem.* **2011**, *32*, 1456.
[49] H. J. Monkhorst, J. D. Pack, *Phys. Rev. B* **1976**, *13*, 5188.
[50] R. Resta, *Rev. Mod. Phys.* **1994**, *66*, 899.
[51] R. D. King-Smith, D. Vanderbilt, *Phys. Rev. B* **1993**, *47*, 1651.